

Temperature and Solvent Effects on H₂ Splitting and Hydricity: Ramifications on CO₂ Hydrogenation by a Rhenium Pincer Catalyst

Jenny Hu,[‡] Quinton J. Bruch,[‡] and Alexander J. M. Miller*

Department of Chemistry, University of North Carolina at Chapel Hill, Chapel Hill, North Carolina 27599–3290, United States

ABSTRACT: The catalytic hydrogenation of carbon dioxide holds immense promise for applications in sustainable fuel synthesis and hydrogen storage. Mechanistic studies that connect thermodynamic parameters with the kinetics of catalysis can provide new understanding and guide predictive design of improved catalysts. Reported here are thermochemical and kinetic analyses of a new pincer-ligated rhenium complex (^tBuPOCOP)Re(CO)₂ (^tBuPOCOP = 2,6-bis(di-*tert*-butylphosphinito)phenyl) that catalyzes CO₂ hydrogenation to formate with faster rates at lower temperature. Because the catalyst follows the prototypical “outer sphere” hydrogenation mechanism, comprehensive studies of temperature and solvent effects on the H₂ splitting and hydride transfer steps are expected to be relevant to many other catalysts. Strikingly large entropy associated with cleavage of H₂ results in a strong temperature dependence on the concentration of [(^tBuPOCOP)Re(CO)₂H][−] present during catalysis, which is further impacted by changing the solvent from toluene to tetrahydrofuran to acetonitrile. New methods for determining the hydricity of metal hydrides and formate at temperatures other than 298 K were developed, providing insight into how temperature can influence the favorability of hydride transfer during catalysis. These thermochemical insights guided the selection of conditions for CO₂ hydrogenation to formate with high activity (up to 364 h^{−1} at 1 atm or 3330 h^{−1} at 20 atm of 1:1 H₂ CO₂). In cases where hydride transfer is the highest individual kinetic barrier, entropic contributions to outer sphere H₂ splitting lead to a unique temperature dependence: *catalytic activity increases as temperature decreases* in tetrahydrofuran (200-fold increase upon cooling from 50 to 0 °C) and toluene (4-fold increase upon cooling from 100 to 50 °C). Ramifications on catalyst structure–function relationships are discussed, including comparisons between “outer sphere” mechanisms and metal–ligand cooperation mechanisms.

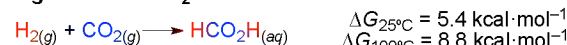
1. INTRODUCTION

Hydrogenation reactions are ubiquitous in chemistry, with industrial applications in pharmaceutical synthesis, commodity chemicals manufacturing, and fuel generation. The hydrogenation of CO₂ to formate or formic acid has attracted particularly intense interest in the context of carbon fixation and liquid fuel synthesis.¹ Efficient CO₂ hydrogenation often requires elevated temperatures, even though entropic penalties render the overall reaction more unfavorable with increasing temperature (Scheme 1A, see SI for thermochemical details). This could be due to a high kinetic barrier under ambient conditions; however, a distinct possibility is that an individual step in the cycle becomes thermodynamically unfavorable at low temperature. Mechanistic studies that connect kinetic and thermodynamic analysis could elucidate the factors that control the temperature dependence of CO₂ hydrogenation.

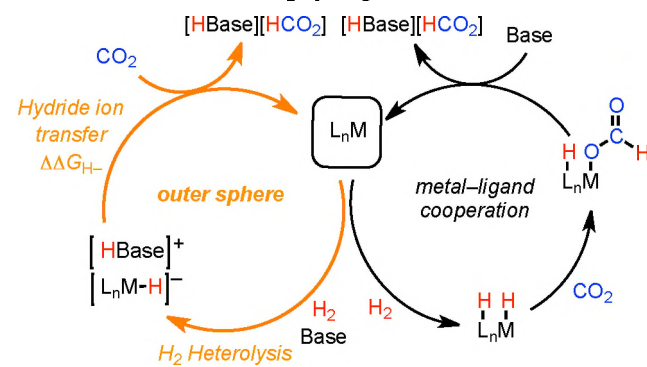
Two general mechanisms, shown in Scheme 1B, are frequently proposed in leading hydrogenation catalysts.^{1–8} The mode of H₂ splitting is distinct in these two mechanisms: the “outer sphere” mechanism utilizes an external base to produce a monohydride in a formally termolecular reaction (sometimes involving two sequential bimolecular steps).^{3,4} Conversely, in the metal–ligand cooperation mechanism a basic site on the ligand is proposed to assist in the heterolytic cleavage of H₂ to form a monohydride and a protonated ligand.^{5,7,8} Enthalpy and entropy of reaction parameters have been determined for a few catalysts that split H₂ via the metal–ligand cooperative mechanism.^{9–11} However, to our knowledge no analogous temperature-dependent thermochemical data is available for the H₂ heterolysis step (ΔG_1) in catalysts that follow an outer sphere mechanism, precluding comparisons between mechanisms.

Scheme 1. Thermodynamic analysis of CO₂ hydrogenation.

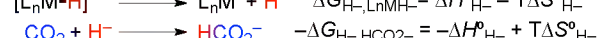
A. Hydrogenation of CO₂ to formic acid or formate in water



B. Two mechanisms of CO₂ hydrogenation



C. Relating hydricity (ΔG_{H^-}) to hydride ion transfer



After H₂ heterolysis, the subsequent C–H bond-forming steps are often also different between the two mechanisms of Scheme 1B. In metal–ligand cooperative pathways, concerted hydride and proton transfer to CO₂ is often invoked, although CO₂ binding and migratory insertion or other mechanisms are also possible.^{5,7} In the outer sphere pathway, the H₂-derived hydride undergoes hydride ion transfer to free CO₂, generating formate ion. When formate does not bind to the catalyst, the thermodynamics of hydride transfer can be directly related to the difference in hydricity (ΔG_{H^-}) between the metal hydride intermediate and the free formate ion

(Scheme 1C, $\Delta\Delta G_{\text{H}_2}$).¹² Thermodynamic hydricity values have been determined for a wide variety of transition metal hydrides in MeCN.^{12,13} However, MeCN is rarely used in CO₂ hydrogenation catalysis. The first hydricity values in tetrahydrofuran (THF), a solvent commonly used in hydrogenation studies, have only very recently appeared.^{10,13,14} Irrespective of solvent, so far $\Delta G_{\text{H}_2}^{\circ}$ -values have only been reported at the standard state temperature of 25 °C, where few catalysts operate.

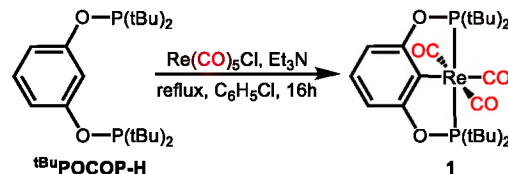
To connect the temperature-dependent thermochemistry of H₂ splitting and hydride transfer steps to overall catalytic CO₂ hydrogenation activity, we set out to prepare a new catalyst that would be amenable to detailed thermochemical studies across a range of temperatures and solvents. We hypothesized that a pincer rhenium carbonyl hydride anion would be a promising catalyst candidate, based on several trends in thermodynamic hydricity.¹³ First, early metal hydrides are often more hydridic than late metal hydrides (stronger hydride donors with lower $\Delta G_{\text{H}_2}^{\circ}$ -values).^{12,13} Second, anionic hydride complexes tend to be more hydridic than neutral or cationic hydride complexes.¹² Third, complexes with a hydride sitting across from a strong *trans* effect ligand (CO in this case) can be more potent hydride donors.^{15–17} Rhenium complexes, including pincer complexes, can catalyze the hydrogenation of organic carbonyls,^{18–23} we are not aware of examples of Re catalysts for CO₂ hydrogenation.¹⁶ We also anticipated an outer sphere hydrogenation mechanism based on the octahedral geometry with 18 valence electrons and the negative charge on the complex.

Herein we report a new rhenium pincer catalyst for CO₂ hydrogenation that provides a platform for understanding how temperature and solvent affect formate synthesis by outer sphere mechanisms. Thermodynamic studies of the temperature dependence of H₂ heterolysis in a variety of solvents reveal striking entropic contributions to the hydride formation step. Insight into the formate-producing hydride transfer step comes from new methods for the determination of temperature-dependent thermodynamic hydricity. Kinetic studies of catalytic activity revealed conditions where the new catalyst *produces formate at higher rates at lower temperatures* in THF and toluene. Mechanistic models that connect the thermodynamic and kinetic factors that enable improved reactivity at low temperature are introduced, and implications on designing future catalyst systems are considered.

2. RESULTS AND DISCUSSION

Synthesis of Rhenium Carbonyl Complexes. A rhenium(I) carbonyl complex supported by the anionic pincer ligand ^tBuPOCOP (2,6-bis(di-*tert*-butylphosphonito)phenyl) was prepared by refluxing ^tBuPOCOP-H with Re(CO)₅Cl and triethylamine in chlorobenzene for 16 h (Scheme 2). Analytically pure, colorless crystals of (^tBuPOCOP)Re(CO)₃ (**1**) were obtained upon cooling a saturated pentane solution to -30 °C. The structure of **1** was ascertained through NMR and IR spectroscopy (ν_{CO} 2023, 1923, and 1902 cm⁻¹) and a single-crystal X-ray diffraction study (Figure 1). The structural metrics and vibrational spectra are similar to related pincer Re carbonyl complexes.^{24–28}

Scheme 2. Synthesis of tricarbonyl complex (^tBuPOCOP)Re(CO)₃ (**1**).



In order to open a coordination site for H₂ activation and hydride formation, carbonyl ligand removal methods were explored. Heating colorless solid **1** at 200 °C under vacuum for 5 h led to sublimation of a dark orange-brown solid that was isolated and found by NMR spectroscopy to feature a new species with a ³¹P resonance shifted downfield by over 20 ppm relative to **1** (which was still present as a 27% impurity). This new species showed just two stretches by IR spectroscopy (ν_{CO} 1910, 1840 cm⁻¹), consistent with formation of (^tBuPOCOP)Re(CO)₂ (**2**).^{25,29} A single-crystal X-ray diffraction study confirmed the formula as the anticipated dicarbonyl complex in a square pyramidal geometry (Figure 1). Evidence for **2** having stronger π -backbonding than **1** comes from crystallographic data (shorter Re–C bonds in **2**) and IR data (lower-energy CO stretches for **2**). The solid-state structure of **2** has pseudo-C₃s molecular symmetry, while the same complex exhibits pseudo-C_{2v} symmetry in solution, perhaps reflecting a rapid isomerization or other structural fluxionality.²⁵

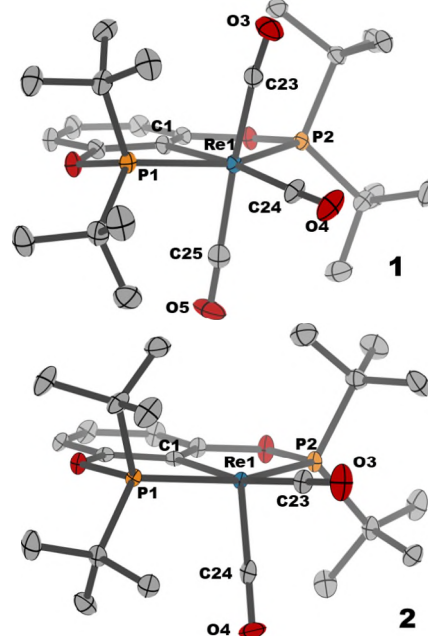


Figure 1. Structural representations of (^tBuPOCOP)Re(CO)₃ (**1**, top) and (^tBuPOCOP)Re(CO)₂ (**2**, bottom) from single crystal x-ray diffraction (ellipsoids are set at 50%, hydrogen atoms omitted for clarity). See SI Section X for crystallographic details.

Isolation of five-coordinate **2** in high purity was essential for subsequent studies of H₂ heterolysis. Therefore, an alternative, two-step decarbonylation strategy was designed based on initial hydride formation followed by protonolysis to afford **2**. We hypothesized that hydride transfer to complex **1** would result in a formyl complex

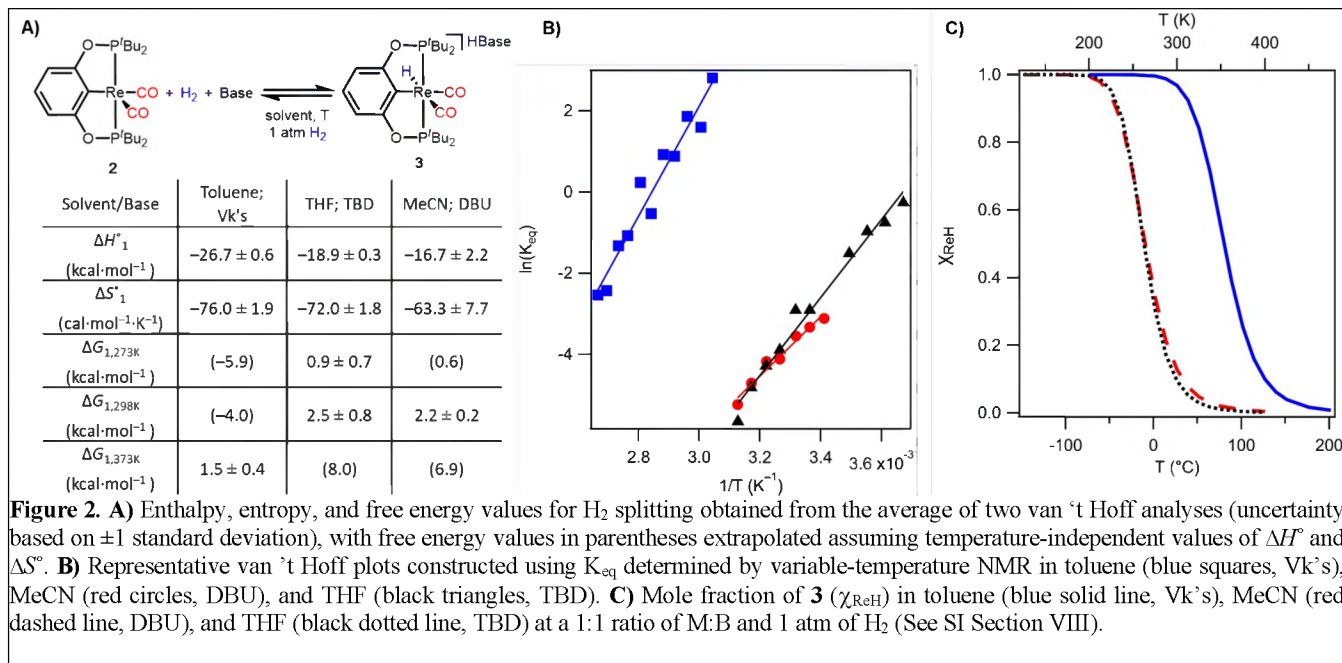
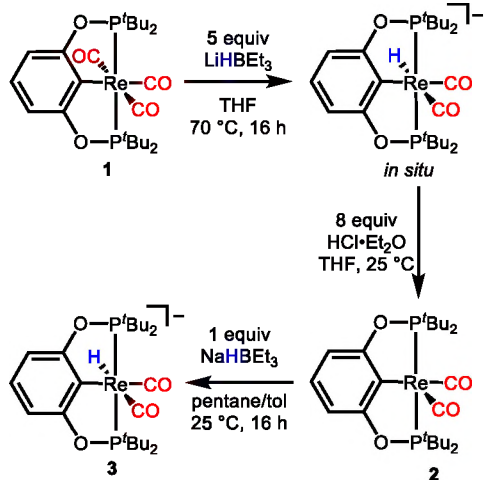


Figure 2. **A)** Enthalpy, entropy, and free energy values for H_2 splitting obtained from the average of two van 't Hoff analyses (uncertainty based on ± 1 standard deviation), with free energy values in parentheses extrapolated assuming temperature-independent values of ΔH° and ΔS° . **B)** Representative van 't Hoff plots constructed using K_{eq} determined by variable-temperature NMR in toluene (blue squares, VK's), MeCN (red circles, DBU), and THF (black triangles, TBD). **C)** Mole fraction of **3** (χ_{ReH}) in toluene (blue solid line, VK's), MeCN (red dashed line, DBU), and THF (black dotted line, TBD) at a 1:1 ratio of M:B and 1 atm of H_2 (See SI Section VIII).

that would release CO and undergo α -migration to form a hydride complex (although other mechanisms are possible).^{30–33} Treating the hydride with acid in the absence of CO would then release H_2 and form **2**. Heating tricarbonyl **1** with 5 equiv LiHBEt₃ (1 M in THF) at 70 °C led to formation of a rhenium hydride species (**Scheme 3**, SI Figure S11). After removal of free CO via freeze-pump-thaw cycling, addition of HCl etherate led to vigorous H_2 evolution as the colorless solution turned dark brown. Dicarbonyl **2** was isolated in >99% purity by this method, based on multinuclear NMR spectroscopy and elemental analysis.

Scheme 3. Synthesis of dicarbonyl complex (^tBuPOCOP)Re(CO)₂ (**2**) and hydride complex [(^tBuPOCOP)Re(CO)₂H]⁻ (**3**).



Attempts to isolate the hydride intermediate proved challenging, as decomposition was always observed during workup due to instability to vacuum and extreme sensitivity to trace moisture. We found it most efficient to treat **2** with 1 equiv of NaHBEt₃ (1 M in toluene) in toluene, followed by precipitation with pentane. The isolated solid displayed a hydride ¹H resonance at -6.13 ppm with strong J_{PH} coupling (25.8 Hz) in freshly dried THF-*d*₈. The molecule exhibited *C*₅ symmetry, as reflected in two distinct *tert*-butyl resonances, indicating a *cis* dicarbonyl geometry (further buttressed by IR spectra showing two carbonyl stretches, ν_{CO} 1873

and 1754 cm⁻¹) and allowing assignment as *cis*-[^tBuPOCOP]Re(CO)₂H⁻ (**3**, **Scheme 3**).

Temperature and Solvent Effects on the Free Energy of H_2 Heterolysis, ΔG_1 . Five-coordinate complex **2** and hydride **3** were considered likely catalytic intermediates that could plausibly be interconverted by an H_2 splitting reaction with exogenous base. Three organic solvents were selected for reactivity and thermochemistry studies: toluene, THF, and MeCN. These solvents not only span a range of polarity and donor ability, but THF and toluene are commonly employed in catalysis and were the solvents used in thermodynamic studies of H_2 splitting by metal-ligand cooperative systems.^{10,11} While MeCN is not often employed in hydrogenation catalysis, it is a classic solvent for thermochemical studies.^{12,34,35}

Solutions of dicarbonyl **2** and various organic bases were prepared in each of the three solvents and placed under 1 atm H_2 to probe for hydrogen cleavage reactivity. In the presence of NEt₃, no reaction was observed in toluene, THF, or MeCN (though spectroscopic evidence for MeCN binding can be observed, see SI Figure S6). In fact, no evidence for H_2 binding was observed even when solutions of **2** in toluene-*d*₈ under 1 atm H_2 were cooled from 298 K to 198 K and monitored by NMR spectroscopy. This indicates that H_2 coordination to **2** is substantially endergonic (SI Figure S21–S22).

We hypothesized that a stronger base than NEt₃ might better facilitate outer sphere H_2 splitting, even though a stable dihydrogen complex was not observed.^{12,13} Indeed, evidence for heterolytic H_2 cleavage and formation of **3** was observed with stronger bases (**Figure 2A**). In MeCN-*d*₈, DBU (1,8-diazabicyclo[5.4.0]undec-7-ene) proved to be the ideal base, producing equilibrium mixtures of **2** and **3** under 1 atm H_2 (see SI Section VI for more details). In tetrahydrofuran-*d*₈, H_2 splitting with TBD (1,5,7-triazabicyclo[4.4.0]dec-5-ene) produced a similar equilibrium mixture. In toluene-*d*₈ at 25 °C, Verkade's base (VK's, 2,8,9-triisobutyl-2,5,8,9-tetraaza-1-phosphabicyclo[3.3.3]undecane) furnished complete conversion of brown **2** to colorless **3**; however, the solution color turned brown upon heating, indicating access to the desired equilibrium at higher temperatures.

Having identified appropriate conditions for equilibrium H_2 cleavage, the temperature dependence of hydride formation in each

solvent was investigated. Teflon-sealed NMR tubes were charged with dicarbonyl complex **2** and the appropriate base in the solvent of interest, filled with 1 atm H₂, and the equilibrium constants were determined by variable-temperature (VT) NMR spectroscopy. The temperature ranges were selected based on the ability to detect all species by NMR spectroscopy and by the solvent boiling points.

Figure 2 shows the van 't Hoff plots (**Figure 2B**) resulting from the variable temperature studies, from which the enthalpy of reaction (ΔH°_1) and entropy of reaction (ΔS°_1) for H₂ heterolysis were obtained in each solvent (**Figure 2A**). Each H₂ splitting reaction is exothermic, ΔH°_1 ranging between -17 and -27 kcal·mol⁻¹. The ΔS°_1 values are strikingly large and negative, reflecting an entropic penalty associated with conversion of three neutral species to two solvated ions. The reaction becomes more entropically unfavorable as the solvent polarity decreases, suggesting that the ions are more tightly paired (more highly ordered) in the less polar solvents.

The enthalpy and entropy terms for this outer sphere H₂ splitting reaction can be compared to other systems that cleave H₂. Outer sphere H₂ splitting by the main group "frustrated" Lewis pair B(C₆F₅)₃/P(tBu)₃ has $\Delta H^\circ_1 = -31.4$ kcal·mol⁻¹ in bromobenzene.³⁶ This value is similar to the enthalpy of H₂ splitting by **2** and V_k's in toluene ($\Delta H^\circ_1 = -26.7$ kcal·mol⁻¹). Metal-ligand cooperative examples include 1,2-addition of H₂ across Fe–N or Fe–B bonds ($\Delta H^\circ_1 \approx -9$ kcal·mol⁻¹ in toluene¹¹ or benzene⁹) and 1,3-addition of H₂ in (PNP*)RuH(CO) ($\Delta H^\circ_1 = -17.4$ kcal·mol⁻¹ in THF; PNP* = 2-(Bu₂PCH₂)-6-(Bu₂PCH)-C₅H₃N).¹⁰

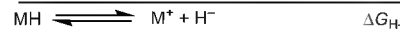
The entropy of H₂ splitting by **2** is far more unfavorable than any comparable systems reported in the literature. The ΔS°_1 of **2** varies from -63.3 cal·mol⁻¹·K⁻¹ in MeCN to -76.0 cal·mol⁻¹·K⁻¹ in toluene. For comparison, the entropy of metal-ligand cooperative 1,3-addition of H₂ is reported ($\Delta S^\circ_1 = -45$ cal·mol⁻¹·K⁻¹ in THF¹⁰) and the 1,2-addition examples are less unfavorable ($\Delta S^\circ_1 = -10$ cal·mol⁻¹·K⁻¹ in toluene¹¹ or -28 cal·mol⁻¹·K⁻¹ benzene⁹). Even the termolecular "frustrated" Lewis pair, for which only a computationally-derived estimate is available, only has an entropic penalty of -56 cal·mol⁻¹·K⁻¹ in bromobenzene.¹²

The highly unfavorable entropy term associated with H₂ splitting by **2** leads to a strong temperature dependence in the formation of hydride complex **3**. Furthermore, because ΔH°_1 and ΔS°_1 vary across the three solvents studied, distinct temperature effects can be expected for each solvent. To visualize the influence of temperature and solvent on the concentration of hydride **3** present in solution, the values of ΔH°_1 and ΔS°_1 were used (assuming temperature independence) to calculate the mole fraction of **3** (χ_{ReH}) as a function of temperature at 1 atm of H₂ and a 1:1 ratio of M:B (see SI Section VIII for derivation). As shown in **Figure 2C** and observed experimentally in VT NMR spectroscopic studies, hydride **3** is dominant at low temperature, while dicarbonyl **2** dominates at high temperature. This indicates that if the kinetic barriers remain surmountable, *catalysis may proceed faster at lower temperatures*. Further changes in reaction conditions such as base identity (pK_a), ratio of base:metal concentrations, or H₂ pressure all impact the χ_{ReH} plot (see SI section VIII for more details).

Solvent Effects on Thermodynamic Hydricity, $\Delta G^\circ_{\text{H}_-}$. We next turned our attention to understanding the thermodynamics of the hydride transfer step. As shown in **Scheme 1C** above, the favorability of hydride transfer is dictated by the difference in hydricity between formate and the hydride donor of interest. The hydricity of **3** was therefore experimentally determined. The H₂

heterolysis method of **Scheme 4** is built on ΔG_1 , so the thermodynamic measurements of the preceding section could be used directly in constructing a thermochemical cycle for hydricity.

Scheme 4. Determination of hydricity through heterolysis of H₂.¹²



MeCN was examined first to enable valuable comparisons with other hydride complexes.^{12,37,38} Using ΔG°_1 (° denotes the standard state temperature of 298 K) from **Figure 2A**, the free energy of protonation, ΔG°_2 , and the H₂ heterolysis constant in MeCN, $\Delta G^\circ_{\text{H}_2}$ (76.0 kcal·mol⁻¹),¹² the thermochemical cycle of **Scheme 4** was used to determine the hydricity of **3** in MeCN at 25 °C ($\Delta G^\circ_{\text{H}_-} = 40.6 \pm 1.0$ kcal·mol⁻¹, **Table 1**). We estimate that the uncertainty of all hydricity values is ± 1 kcal·mol⁻¹, which is derived from the uncertainty in the reduction potentials needed to establish the reference hydricity scales (the experimental uncertainty based on our own K_{eq} measurements was smaller, see Figures S17-S18).¹²

Table 1. Hydricity ($\Delta G^\circ_{\text{H}_-}$) of **3** in THF and MeCN at 298 K.

Solvent	Base (pK _a) ³⁹	$\Delta G^\circ_{\text{H}_-}$ (kcal·mol ⁻¹)
THF	TBD (21.0)	37.6 ± 1.0
MeCN	DBU (24.3)	40.6 ± 1.0

Rhenium hydride **3** is a potent hydride donor in MeCN: hydride transfer from **3** to CO₂ is thermodynamically favored by ca. 3 kcal·mol⁻¹ ($\Delta G^\circ_{\text{H}_-}$ ca. 44 kcal·mol⁻¹ for HCO₂⁻).¹² Although hydricity studies of other rhenium hydride complexes are lacking, **3** is ca. 5-7 kcal·mol⁻¹ more hydridic than the neutral Mn tricarbonyl hydrides with substituted bipyridine ligands.⁴⁰ Hydride **3** is similarly hydridic to the anionic group 6 hydride [W(CO)₅H]⁻.¹²

The hydricity of **3** was also determined in THF. Using ΔG°_1 from **Figure 2A**, along with the recently reported value of $\Delta G^\circ_{\text{H}_2}$ (68.7 kcal·mol⁻¹),¹⁴ the hydricity in THF at 25 °C was determined ($\Delta G^\circ_{\text{H}_-} = 37.6 \pm 1.0$ kcal·mol⁻¹, **Table 1**). Hydricities in THF have not been reported until recently.^{10,13} Comparing the hydricity of hydrides in THF (see Table S1 in the SI), complex **3** is more hydridic than neutral (PNP)Ru(H₂)(CO) ($\Delta G^\circ_{\text{H}_-}$ in THF = 44.6 kcal·mol⁻¹; PNP = 2,6-bis(Bu₂PCH₂)-C₅H₃N), and falls in the range of anionic bimetallic cobalt hydrides.^{10,13} On the basis of an estimated hydricity of formate in THF and the known catalytic activity of anionic bimetallic cobalt hydrides,^{10,13,41} complex **3** should also be sufficiently hydridic to produce formate from hydride transfer to CO₂ in THF.

To confirm this hypothesis, **3** was generated *in situ* in THF-*d*₈ by addition of LiHBET₃ to **2** and subsequently placed under an atmosphere of CO₂ (1 atm). Complete conversion of **3** to the five-coordinate complex **2** (as well as <5% tricarbonyl complex **1**) was accompanied by the formation of free formate (δ 8.22 by ¹H NMR, see SI Figure S19-S20). The lack of formate binding simplifies the situation, as the thermodynamics of ligand binding need not be considered. Considering that hydride complex **3** is an octahedral complex with a valence electron count of 18 and that formate does not coordinate after hydride transfer, an outer sphere hydride ion transfer is highly likely. A seminal study of *fac*-Re(bpy)(CO)₃H was also consistent with an outer sphere pathway.⁴²

The lack of a defined pK_a scale in toluene and available thermochemical data to determine $\Delta G_{H_2}^{\circ}$ precluded the determination of hydricity in toluene.

Temperature Effects on Thermodynamic Hydricity, ΔG_{H^-} . To date, thermodynamic hydricity values have only been determined at 298 K. Determining the temperature-dependent hydricity (ΔG_{H^-}) requires knowledge of the temperature dependence of outer sphere H_2 splitting, the acidity of the external acid/base pair, and the heterolysis of free H_2 . We developed a thermochemical methodology that sums the free energy of each reaction in **Scheme 4** at a given temperature, focusing on MeCN solvent based on the availability of thermodynamic parameters.

The free energy of H_2 heterolysis, ΔG_1 , was available from 293 to 320 K from VT NMR equilibrium studies (**Figure 2**). The pK_a of DBU was assumed to be temperature-independent, based on studies of nitrogen heterocycles in MeCN.^{43,44} Although the pK_a change is likely negligible, ΔG_2 decreases by 3 kcal·mol⁻¹ as the temperature increases over the studied range (SI Table S3). The temperature-dependent free energy of H_2 heterolysis, ΔG_{H_2} , was estimated based on the free energy of H^+ reduction to H^- in water at a given temperature (based on temperature-dependent reduction potential data),⁴⁵ coupled with the ion transfer free energy of H^+ and H^- from water to MeCN at the same given temperature (see SI Section VII for derivation). ΔG_{H_2} increases as a function of temperature (see SI Table S3 and Figure S30).

Summing ΔG_1 , ΔG_2 , and ΔG_{H_2} at a given temperature enabled the determination of the hydricity of complex **2** at that temperature. Hydride **3** becomes more hydridic (smaller ΔG_{H^-} values) with increasing temperature over the experimental range of 293 to 320 K in MeCN (**Figure 3**, red triangles). Enthalpy and free energy measurements of organic hydride donors and a few transition hydrides at 298 K predict a decrease in ΔG_{H^-} with increasing temperature.^{12,46,47} This new thermochemical methodology enabled the first experimental validation of this prediction and provides a quantitative estimate of the temperature dependence of hydricity.

To gain insight into how temperature influences the thermodynamics of hydride transfer from **3** to CO_2 , which is a key step in CO_2 hydrogenation, the temperature dependence of the hydricity of formate is needed. We therefore additionally developed a thermochemical cycle to determine ΔG_{H^-} for formate in MeCN (see SI Section VII for derivation). The hydricity of formate was found to be significantly less sensitive to temperature (**Figure 3**, blue squares). **Figure 3** shows that hydride transfer from **3** to CO_2 is thermodynamically favorable over the full temperature range studied in MeCN. Assuming a linear temperature dependence, the data can be extrapolated to predict that this favorability will be maintained above -12 °C. Hydride transfer to CO_2 becomes more exergonic as the temperature increases in MeCN.

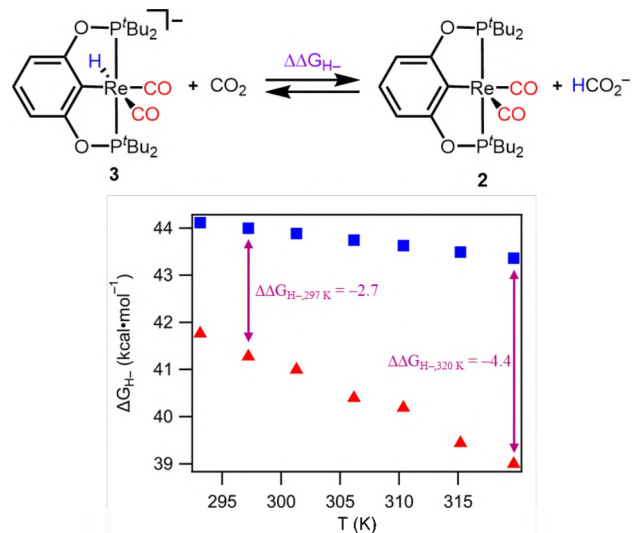
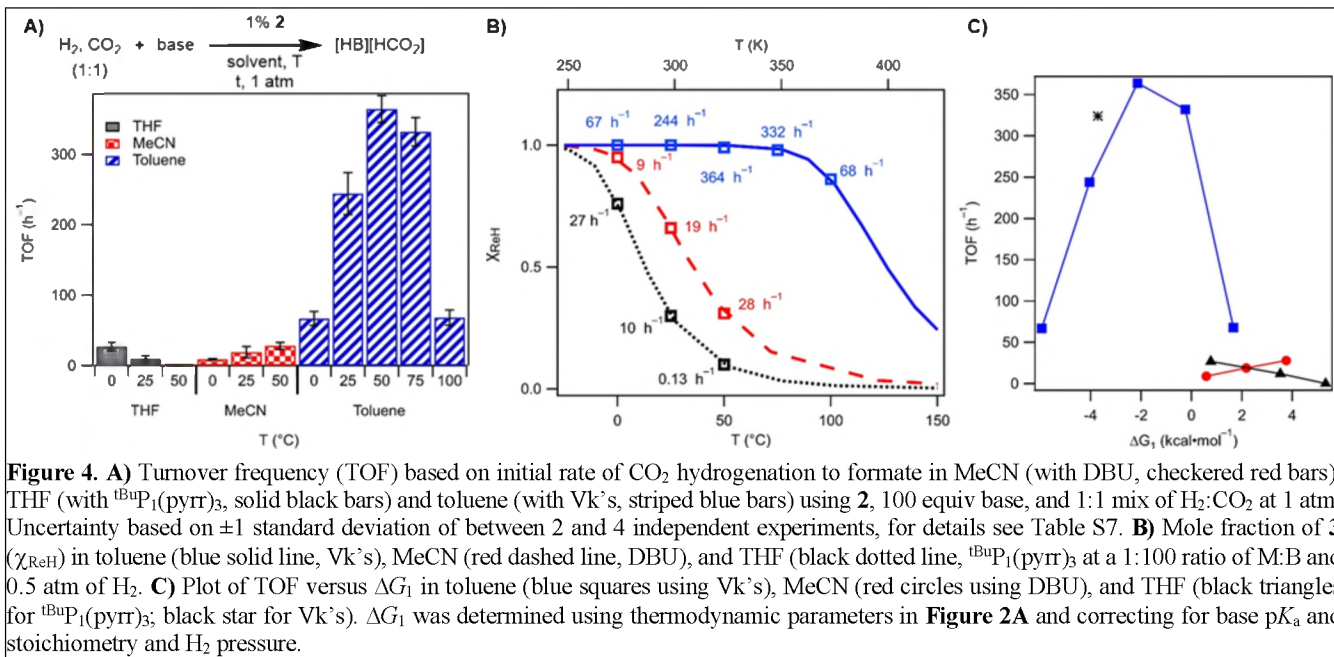


Figure 3. Plot of ΔG_{H^-} of **3** (red triangles) and HCO_2^- (blue squares) as well as $\Delta\Delta G_{H^-}$ for hydride transfer from **3** to CO_2 (purple arrows) in acetonitrile.

Hydrogenation of CO_2 to Formate: Thermochemistry-Guided Development of Catalytic Conditions. The H_2 splitting and hydride transfer reactivity observed in the preceding thermochemical studies constitute the individual steps of CO_2 hydrogenation catalysis via an “outer sphere” type mechanism (**Scheme 1** above). The two-step outer sphere mechanism would facilitate direct connections between thermodynamic parameters and the kinetics of catalysis. We therefore carried out catalytic CO_2 hydrogenation studies over a wide range of temperatures in three solvents. Catalytic CO_2 hydrogenation activity was assessed using the turnover frequency (TOF, defined as moles of formate divided by moles of catalyst and the reaction time), based on initial rates (<10% conversion) of CO_2 hydrogenation under 1 atm 1:1 H_2 : CO_2 . Conditions aligned with the thermodynamic studies whenever possible to facilitate comparisons with experimental thermodynamic data. Additionally, using the weakest bases possible minimizes excess driving force in the reaction; a key parameter in liquid fuel synthesis or H_2 storage.^{1,6,48}

In THF, dicarbonyl complex **2** and 100 equivalents of $^{t\text{Bu}}\text{P}_1(\text{pyrr})_3$ (pyrr = pyrrolidinyl, $pK_a = 20.3$ in THF⁴⁹) were allowed to react with H_2 and CO_2 at 0 °C, 25 °C, and 50 °C. The base $^{t\text{Bu}}\text{P}_1(\text{pyrr})_3$ was chosen as a more soluble alternative to TBD with a similar pK_a value. As shown in **Figure 4A**, the catalytic activity exhibits a striking temperature dependence: *the reaction becomes ca. 200-fold faster as the temperature is decreased* (TOF = $27 \pm 6 \text{ h}^{-1}$ at 0 °C and $0.13 \pm 0.06 \text{ h}^{-1}$ at 50 °C). The almost complete loss of catalytic activity at 50 °C is in line with the predicted low



concentration of **3** ($\chi_{\text{ReH}} = 0.10$ at 50 °C; **Figure 4B**) resulting from uphill H_2 splitting thermodynamics ($\Delta G_1 = 5.4 \text{ kcal}\cdot\text{mol}^{-1}$). At 0 °C, where a high concentration of **3** is predicted ($\chi_{\text{ReH}} = 0.76$) and H_2 splitting is almost ergoneutral ($\Delta G_1 = 0.8 \text{ kcal}\cdot\text{mol}^{-1}$), catalysis can proceed — the kinetic barriers remain surmountable at this temperature. Catalyst activity varied linearly with the change in favorability of H_2 splitting, ΔG_1 , as shown in **Figure 4C**, suggesting that H_2 splitting is influencing the rate limiting step (see below for further details). While faster net hydride ion transfer at lower temperatures has been observed for organohydride donors, we are not aware of any such examples in catalytic CO_2 hydrogenation.^{50,51}

If H_2 splitting is involved in the turnover-limiting step(s), a stronger base should accelerate the reaction. Using V_k 's base (estimated $\text{p}K_a$ of 26.6 in THF)⁵² in THF would shift ΔG_1 at 50 °C from +5.4 $\text{kcal}\cdot\text{mol}^{-1}$ (with ${}^{\text{tB}}\text{P}_1(\text{pyrr})_3$) to $-3.9 \text{ kcal}\cdot\text{mol}^{-1}$, increasing χ_{ReH} from 0.1 to ca. 1.0). As predicted, CO_2 hydrogenation at 50 °C in THF proceeded faster with V_k 's base when compared with ${}^{\text{tB}}\text{P}_1(\text{pyrr})_3$ (increased from $0.13 \pm 0.06 \text{ h}^{-1}$ to $324 \pm 8 \text{ h}^{-1}$).

In MeCN containing 100 equiv DBU, catalyst **2** exhibits the opposite temperature dependence. The reaction is slow at 0 °C (TOF = $9 \pm 1 \text{ h}^{-1}$), and the rate increases slightly as the temperature increases to 50 °C (TOF = $28 \pm 5 \text{ h}^{-1}$, **Figure 4**). We propose that H_2 splitting becomes the turnover-limiting step in MeCN due to solvent binding (*vide supra*) that inhibits H_2 binding and activation. Consistent with slow H_2 association, the use of a stronger base (V_k 's, $\text{p}K_a = 33.5$ ⁵³, 8.2 $\text{p}K_a$ units stronger than DBU) did not change the initial TOF at 50 °C ($28 \pm 5 \text{ h}^{-1}$ with DBU versus $32 \pm 8 \text{ h}^{-1}$ with V_k 's). Correlations with $\Delta \Delta G_{\text{H}_2}$ are consistent with pre-equilibrium contributions to rate, but we propose that the TOF temperature dependence is dominated by H_2 binding (see below for further details).

In toluene containing 100 equiv V_k 's base, catalyst **2** operates with higher TOF values in comparison to THF or MeCN at all temperatures examined. This broadly correlates with predictions, given that H_2 splitting was most favorable in toluene and the highest concentration of hydride **3** is predicted in this solvent. Differences in CO_2 solubility in each solvent represents an alternative explanation for the differences in activity, but

comparing TOF across solvents under otherwise identical conditions using V_k 's base showed no correlation with CO_2 solubility; in fact, the highest TOF was observed in toluene, where CO_2 is least soluble (ca. 0.05 M at 0.5 atm and 298 K; c.f. ca. 0.14 M in THF and MeCN).⁵⁴ Interestingly, in comparison to the linear temperature-dependent behavior observed in THF and MeCN, a distinct temperature dependence profile was observed in toluene. A maximum in activity is observed at 50 °C (TOF = $364 \pm 18 \text{ h}^{-1}$), with slower rates at both lower and higher temperatures (**Figure 4**). During investigations of the catalyst stability by NMR spectroscopy, no decomposition was observed after 24 h at 25 °C and only 13% conversion to tricarbonyl **1** after 11 h at 50 °C (SI Figure S43). This suggests that catalyst decomposition is unlikely to affect the initial TOF reactivity (collected within 5 min in most cases).

The initial rates TOF of CO_2 hydrogenation in toluene at ambient temperature of 244 h^{-1} at only 0.5 atm each of H_2 and CO_2 compares favorably with other CO_2 -to-formate hydrogenation catalysts (Table S7-8 in the SI). Increasing from 1 atm to 20 atm 1:1 $\text{CO}_2:\text{H}_2$ leads to a 14-fold increase in rate, TOF = $3330 \pm 340 \text{ h}^{-1}$ (see SI Section IX). Running catalysis to full conversion at 25 °C and 1 atm of 1:1 $\text{H}_2:\text{CO}_2$ in toluene with 0.1 mol% **2** and 1,000 equiv V_k 's resulted in a turnover number (TON) of 1023 ± 27 ($102 \pm 3\%$ yield). The final TOF ($227 \pm 6 \text{ h}^{-1}$) was within error of the TOF value from initial rates ($244 \pm 30 \text{ h}^{-1}$), consistent with sustained activity of **2** over extended reaction times and ruling out any significant product inhibition.

A General Model for Understanding the Ramifications of Temperature on Outer Sphere CO_2 Hydrogenation Reactions. Studying both the thermodynamics of individual steps and the kinetics of catalysis in multiple solvents allows us to develop a general mechanistic understanding of how temperature affects outer sphere CO_2 hydrogenation catalysts. In this section, we introduce representative reaction coordinate diagrams (RCDs) and discuss the influence of temperature on the activation barriers and individual reaction free energies. The insights should be generally applicable to other catalysts that follow an outer sphere mechanism.

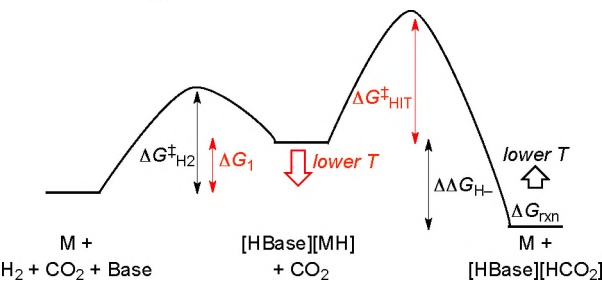
Figure 5 shows two RCDs for outer sphere CO_2 hydrogenation to formate. On the basis of our reactivity and thermodynamic studies,

we adopt a model where ΔG_1 is endergonic and $\Delta\Delta G_{H^-}$ is exergonic. We also adopt the common assumption that any change in barrier heights ΔG^\ddagger with temperature is negligible. The overall reaction, ΔG_{rxn} , must be exergonic in order to proceed to completion. There are two limiting regimes in this experimentally informed model: when the highest single-step barrier height is associated with hydride ion transfer (ΔG^\ddagger_{HIT}), or when it is associated with H_2 splitting (ΔG^\ddagger_{H2}).

Figure 5A shows the case of a larger hydride ion transfer (HIT) barrier, ΔG^\ddagger_{HIT} . With $\Delta G_1 > 0$ kcal·mol⁻¹, TOF will depend on both ΔG_1 and ΔG^\ddagger_{HIT} .⁵⁵ Because outer sphere H_2 splitting to form a metal hydride features a large negative entropy of reaction, ΔG_1 will *decrease dramatically* with decreasing temperature. For catalyst **2** in THF (above 0 °C) and in toluene (above 50 °C), the change in barrier height ($\Delta G_1 + \Delta G^\ddagger_{HIT}$) affects the rate constant more than the change in temperature, *so the TOF increases with decreasing temperature*. Knowing that higher temperatures will not always lead to faster catalysis is a broadly important finding — one that may run counter to expectations,⁵⁶ but that is observed in enzyme catalysis and is readily explained by the pre-equilibrium model of the RCD.

A. Higher TOF at lower T

$$TOF \propto \Delta G_1 + \Delta G^\ddagger_{HIT}$$



B. Lower TOF at lower T

$$TOF \propto \Delta G^\ddagger_{H2} (\Delta\Delta G_{H^-} \text{ large and negative})$$

$$TOF \propto \Delta G^\ddagger_{H2} + \Delta\Delta G_{H^-} (\Delta\Delta G_{H^-} \text{ small})$$

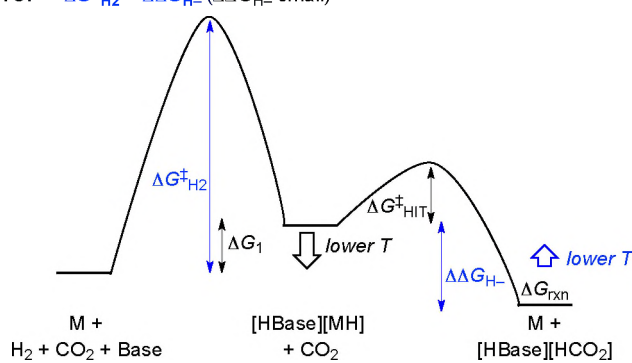


Figure 5. Idealized reaction coordinate diagrams for outer-sphere CO_2 hydrogenation highlighting limiting cases of: (A) high-barrier hydride ion transfer and (B) high-barrier H_2 splitting.

Figure 5B shows the case of a H_2 splitting barrier, ΔG^\ddagger_{H2} , that is larger than ΔG^\ddagger_{HIT} . If $\Delta\Delta G_{H^-}$ is large and negative, the TOF will depend only on ΔG^\ddagger_{H2} and decreasing temperature will decrease the rate. If $\Delta\Delta G_{H^-}$ is small, however, this thermodynamic parameter will also affect the equilibrium concentration of M during turnover and thus influence TOF. For catalyst **2** in MeCN, equilibrium solvent binding to the catalyst is proposed to result in a relatively large ΔG^\ddagger_{H2} barrier (likely composed of both solvent dissociation and H_2 splitting) as shown in **Figure 5B**. Strong correlations

between the TOF of **2** and $\Delta\Delta G_{H^-}$ suggest a pre-equilibrium regime in MeCN. The TOF thus depends on $\Delta\Delta G_{H^-}$ and ΔG^\ddagger_{H2} , but the magnitude of ΔG^\ddagger_{H2} dominates such that TOF decreases with decreasing temperature. Quantitative RCDs in MeCN support this model (SI Figure S45).

For future catalysis studies, simplified qualitative RCDs such as those in **Figure 5** can enable predictions about the expected temperature dependence of the hydrogenation TOF. In fact, the observation of inverse temperature effects (higher TOF at lower temperature) can be taken as a strong mechanistic indicator: only pre-equilibrium H_2 splitting followed by high-barrier hydride transfer is expected to follow such a temperature dependence in outer sphere hydrogenation reactions. Knowledge of the RCD can also enable predictions about when changing H_2 pressure, CO_2 pressure, or base pK_a might influence TOF.

Implications of Thermochemical Data on Catalyst Design. In this section, we compare the outer sphere mechanism with the metal–ligand cooperation mechanism as they relate to catalyst design principles in CO_2 hydrogenation.

The most striking differences are in the entropy of H_2 splitting. The entropy associated with metal–ligand cooperative H_2 heterolysis has been determined for two hydrogenation catalysts. The 1,2-addition of H_2 to (ⁱPrPNP)FeH(CO) in toluene has a small negative entropy term ($\Delta S^\circ_1 = -9.7$ cal·mol⁻¹·K⁻¹, $\Delta H^\circ_1 = -7.8$ kcal/mol; ⁱPrPNP = N(CH₂CH₂P^tPr₂)₂).¹¹ The 1,3-addition of H_2 to (PNP*)RuH(CO) in THF has a somewhat larger negative entropy term ($\Delta S^\circ_1 = -45$ cal·mol⁻¹·K⁻¹, $\Delta H^\circ_1 = -17.4$ kcal/mol).¹⁰ The newly reported thermodynamic data reveals a much larger entropic penalty for outer sphere H_2 splitting, ΔS°_1 of -63.3 to -76.0 cal·mol⁻¹·K⁻¹.

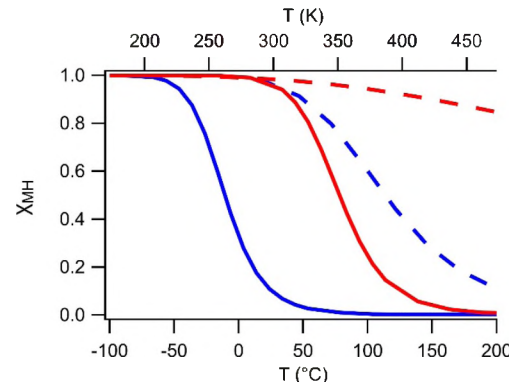


Figure 6. Mole fraction of hydride (χ_{MH}) at 1:1 M:B ratio and 1 atm of H_2 for **3** in toluene (red solid, V_k 's, **3** in THF (blue solid, TBD), (H -ⁱPrPNP)FeH₂(CO) in toluene (red dashed), and (PNP*)Ru(H)₂(CO) in THF (blue dashed).

The entropic differences are reflected in distinct temperature-dependent speciation profiles for catalysts following the two different mechanisms (**Figure 6**). The change in χ_{MH} as a function of temperature is much more gradual for metal–ligand cooperative H_2 splitting than for termolecular outer sphere H_2 heterolysis. This suggests that catalysts following metal–ligand cooperation mechanisms will be less likely to show rate enhancements with decreasing temperature, as the barrier heights could change more than ΔG_1 as a function of temperature. Furthermore, while the temperature-dependence of metal–ligand cooperative H_2 splitting is dictated by the structure of the catalyst, the temperature-

dependence of outer sphere H₂ splitting will depend on the both the catalyst structure and the choice of base.

The distinct temperature-dependent thermochemistry of catalysts that operate via outer sphere mechanisms and those that operate via metal–ligand cooperation has not been recognized previously. The stark differences in temperature-dependent behavior may help chemists identify appropriate catalysts to suit the target application. For example, an outer sphere catalyst that undergoes speciation changes over a very narrow temperature range (tunable by the choice of base) might be ideal for thermally reversible H₂ storage.^{1,6,48}

3. CONCLUSIONS

A new rhenium catalyst for CO₂ hydrogenation to formate via an outer sphere mechanism was the subject of a detailed study connecting the thermodynamics of individual H₂ splitting and hydride transfer steps with the kinetics of catalysis.

The coordinatively unsaturated rhenium complex **2** heterolytically cleaves H₂ with an exogenous base to form hydride complex **3**. The first experimental determination of enthalpy and entropy of an outer sphere H₂ splitting reaction of this kind revealed an extremely large and negative entropy of reaction that varies systematically across three organic solvents. This finding is expected to be representative of the entropy parameters for the many other catalysts known to operate via H₂ splitting with external bases.

The other step in the outer sphere mechanism is hydride ion transfer from the metal hydride intermediate to CO₂, producing the formate anion. The first hydricity measurements of any rhenium hydride revealed a strong hydride donor capable of reducing CO₂ to formate. Further, we have introduced new thermochemical methodology to enable the determination of temperature-dependent hydricity values. The present rhenium hydride complex becomes more hydridic at higher temperatures. Coupled to the distinct temperature dependence of the hydricity of formate, we found that hydride transfer from the rhenium complex to CO₂ becomes increasingly favorable with increasing temperature in acetonitrile.

By connecting thermodynamic parameters with catalytic activity, broadly applicable reaction coordinate diagram models could be constructed that explain the temperature- and solvent-dependent reactivity. The highly unusual temperature effect whereby hydrogenation accelerates as the temperature decreases is attributed to the large entropy associated with termolecular H₂ splitting in a pre-equilibrium preceding hydride ion transfer. This analysis not only shows how thermochemical studies can assist in catalyst development, but sheds light on the salient differences between termolecular systems that undergo base-assisted H₂ heterolysis, and bimolecular systems that feature metal–ligand cooperation.

ASSOCIATED CONTENT

Supporting Information

Experimental details and characterization data (PDF)

Crystallographic data (CIF)

This material is available free of charge via the Internet at <http://pubs.acs.org>.

Accession Codes

Crystallographic data, CCDC 2048210-2048211, can be obtained free of charge via www.ccdc.cam.ac.uk/data_request/cif, or by emailing data_request@ccdc.cam.ac.uk.

AUTHOR INFORMATION

Corresponding Author

* A.J.M.M. Email: ajmm@email.unc.edu

Notes

‡ These co-authors contributed equally.

No competing financial interests have been declared.

ACKNOWLEDGMENT

This work was supported by the U.S. Department of Energy, Office of Science, Office of Basic Energy Sciences, under Award No. DE-SC0014255. J.H. was supported by the J. Thurman Freeze scholarship fund. Q.J.B. acknowledges support from the NSF Graduate Research Fellowship Program (DGE-1650116) and the UNC Dissertation Completion Fellowship program. The authors thank Andrew Camp and Marc ter Horst for assistance with NMR spectroscopy experiments. The mass spectrometry work was supported by the National Science Foundation under Grant No. CHE-1726291. The NMR spectroscopy work was supported by the National Science Foundation under Grant No. CHE-1828183.

REFERENCES

- (1) Sordakis, K.; Tang, C.; Vogt, L. K.; Junge, H.; Dyson, P. J.; Beller, M.; Laurenczy, G. Homogeneous Catalysis for Sustainable Hydrogen Storage in Formic Acid and Alcohols. *Chem. Rev.* **2018**, *118*, 372–433.
- (2) Jessop, P. G.; Ikariya, T.; Noyori, R. Homogeneous Hydrogenation of Carbon Dioxide. *Chem. Rev.* **1995**, *95*, 259–272.
- (3) Clapham, S. E.; Hadzovic, A.; Morris, R. H. Mechanisms of the H₂-Hydrogenation and Transfer Hydrogenation of Polar Bonds Catalyzed by Ruthenium Hydride Complexes. *Coord. Chem. Rev.* **2004**, *248*, 2201–2237.
- (4) Eisenstein, O.; Crabtree, R. H. Outer Sphere Hydrogenation Catalysis. *New J. Chem.* **2013**, *37*, 21–27.
- (5) Khusnutdinova, J. R.; Milstein, D. Metal-Ligand Cooperation. *Angew. Chem. Int. Ed.* **2015**, *54*, 12236–12273.
- (6) Wang, W. H.; Himeda, Y.; Muckerman, J. T.; Manbeck, G. F.; Fujita, E. CO₂ Hydrogenation to Formate and Methanol as an Alternative to Photo- and Electrochemical CO₂ Reduction. *Chem. Rev.* **2015**, *115*, 12936–12973.
- (7) Bernskoetter, W. H.; Hazari, N. Reversible Hydrogenation of Carbon Dioxide to Formic Acid and Methanol: Lewis Acid Enhancement of Base Metal Catalysts. *Acc. Chem. Res.* **2017**, *50*, 1049–1058.
- (8) Dub, P. A.; Gordon, J. C. Metal-Ligand Bifunctional Catalysis: The “Accepted” Mechanism, the Issue of Concertedness, and the Function of the Ligand in Catalytic Cycles Involving Hydrogen Atoms. *ACS Catal.* **2017**, *7*, 6635–6655.
- (9) Harman, W. H.; Peters, J. C. Reversible H₂ Addition across a Nickel-Borane Unit as a Promising Strategy for Catalysis. *J. Am. Chem. Soc.* **2012**, *134*, 5080–5082.
- (10) Mathis, C. L.; Geary, J.; Ardon, Y.; Reese, M. S.; Philliber, M. A.; VanderLinden, R. T.; Saouma, C. T. Thermodynamic Analysis of Metal-Ligand Cooperativity of PNP Ru Complexes: Implications for CO₂ Hydrogenation to Methanol and Catalyst Inhibition. *J. Am. Chem. Soc.* **2019**, *141*, 14317–14328.
- (11) Smith, N. E.; Bernskoetter, W. H.; Hazari, N. The Role of Proton Shuttles in the Reversible Activation of Hydrogen via Metal-Ligand Cooperation. *J. Am. Chem. Soc.* **2019**, *141*, 17350–17360.
- (12) Wiedner, E. S.; Chambers, M. B.; Pitman, C. L.; Bullock, R. M.; Miller, A. J. M.; Appel, A. M. Thermodynamic Hydricity of Transition Metal Hydrides. *Chem. Rev.* **2016**, *116*, 8655–8692.
- (13) Brereton, K. R.; Smith, N. E.; Hazari, N.; Miller, A. J. M. Thermodynamic and Kinetic Hydricity of Transition Metal Hydrides. *Chem. Soc. Rev.* **2020**, *49*, 7929–7948.
- (14) Brereton, K. R.; Jadrich, C. N.; Stratakes, B. M.; Miller, A. J. M. Thermodynamic Hydricity across Solvents: Subtle Electronic Effects and Striking Ligation Effects in Iridium Hydrides. *Organometallics* **2019**, *38*, 3104–3110.
- (15) Furno, F.; Fox, T.; Schmalle, H. W.; Berke, H. 1,2-Bis(Dimethylphosphino)Ethanehydridomesitylidyne-

Tungsten(IV). Hydride Activation via the Trans Influence. *Organometallics* **2000**, *19*, 3620–3630.

(16) Jiang, Y.; Berke, H. Nitrosyl Complexes in Homogeneous Catalysis. *Struct. Bond.* **2014**, *153*, 167–228.

(17) Garg, K.; Matsubara, Y.; Ertem, M. Z.; Lewandowska-Andraloje, A.; Sato, S.; Szalda, D. J.; Muckerman, J. T.; Fujita, E. Striking Differences in Properties of Geometric Isomers of $[\text{Ir}(\text{Ppy})\text{H}]^+$: Experimental and Computational Studies of Their Hydricities, Interaction with CO_2 , and Photochemistry. *Angew. Chem. Int. Ed.* **2015**, *54*, 14128–14132.

(18) Choualeb, A.; Lough, A. J.; Gusev, D. G. Hydridic Rhenium Nitrosyl Complexes with Pincer-Type PNP Ligands. *Organometallics* **2007**, *26*, 3509–3515.

(19) Vogt, M.; Nerush, A.; Diskin-Posner, Y.; Ben-David, Y.; Milstein, D. Reversible CO_2 Binding Triggered by Metal–Ligand Cooperation in a Rhenium(I) PNP Pincer-Type Complex and the Reaction with Dihydrogen. *Chem. Sci.* **2014**, *5*, 2043–2051.

(20) Wei, D.; Roisnel, T.; Darcel, C.; Clot, E.; Sortais, J.-B. Hydrogenation of Carbonyl Derivatives with a Well-Defined Rhenium Precatalyst. *ChemCatChem* **2017**, *9*, 80–83.

(21) Piehl, P.; Peña-López, M.; Frey, A.; Neumann, H.; Beller, M. Hydrogen Autotransfer and Related Dehydrogenative Coupling Reactions Using a Rhenium(I) Pincer Catalyst. *Chem. Commun.* **2017**, *53*, 3265–3268.

(22) Glatz, M.; Stöger, B.; Himmelbauer, D.; Veiro, L. F.; Kirchner, K. Chemoselective Hydrogenation of Aldehydes under Mild, Base-Free Conditions: Manganese Outperforms Rhenium. *ACS Catal.* **2018**, *8*, 4009–4016.

(23) Li, H.; Wei, D.; Bruneau-Voisine, A.; Ducamp, M.; Henrion, M.; Roisnel, T.; Dorcet, V.; Darcel, C.; Carpenter, J.-F.; Soulé, J.-F.; Sortais, J.-B. Rhenium and Manganese Complexes Bearing Amino-Bis(Phosphinite) Ligands: Synthesis, Characterization, and Catalytic Activity in Hydrogenation of Ketones. *Organometallics* **2018**, *37*, 1271–1279.

(24) Radosevich, A. T.; Melnick, J. G.; Stoian, S. A.; Bacciu, D.; Chen, C. H.; Foxman, B. M.; Ozerov, O. V.; Nocera, D. G. Ligand Reactivity in Diarylamido/Bis(Phosphine) PNP Complexes of $\text{Mn}(\text{CO})_3$ and $\text{Re}(\text{CO})_3$. *Inorg. Chem.* **2009**, *48*, 9214–9221.

(25) Vogt, M.; Nerush, A.; Iron, M. A.; Leitus, G.; Diskin-Posner, Y.; Shimon, L. J. W.; Ben-David, Y.; Milstein, D. Activation of Nitriles by Metal Ligand Cooperation. Reversible Formation of Ketimido- and Enamido-Rhenium PNP Pincer Complexes and Relevance to Catalytic Design. *J. Am. Chem. Soc.* **2013**, *135*, 17004–17018.

(26) Kosanovich, A. J.; Reibenspies, J. H.; Ozerov, O. V. Complexes of High-Valent Rhenium Supported by the PCP Pincer. *Organometallics* **2016**, *35*, 513–519.

(27) Rao, G. K.; Korobkov, I.; Gabidullin, B.; Richeson, D. Employing a Neutral “ PN_3P^- ” Pincer to Access Mer-Re(I) Tricarbonyl Complexes: Autoionization of a Halo Ligand and the Role of an N-R (R = H, Me) Substituent. *Polyhedron* **2018**, *143*, 62–69.

(28) Glatz, M.; Pecak, J.; Haager, L.; Stoeger, B.; Kirchner, K. Synthesis and Characterization of Bis- and Tris-Carbonyl $\text{Mn}(\text{I})$ and $\text{Re}(\text{I})$ PNP Pincer Complexes. *Monatshefte für Chemie* **2019**, *150*, 111–119.

(29) Kosanovich, A. J.; Shih, W. C.; Ozerov, O. V. Synthesis and Characterization of Unsaturated Manganese(I) and Rhenium(I) Dicarbonyl Complexes Supported by an Anionic PNP Pincer. *J. Organomet. Chem.* **2019**, *897*, 1–6.

(30) Tam, W.; Lin, G. Y.; Wong, W. K.; Kiel, W. A.; Wong, V. K.; Gladysz, J. A. Synthesis and Electrophile-Induced Disproportionation of the Neutral Formyl ($\eta\text{-C}_5\text{H}_5$) $\text{Re}(\text{NO})(\text{PPh}_3)(\text{CHO})$. *J. Am. Chem. Soc.* **1982**, *104*, 141–152.

(31) Tam, W.; Lin, G. Y.; Gladysz, J. A.; Gladysz, J. A. Syntheses of Kinetically Unstable Neutral Formyl Complexes via $\text{Li}(\text{C}_2\text{H}_5)\text{BH}$ and “Transformylation” Reactions of Metal Carbonyl Cations. *Organometallics* **1982**, *1*, 525–529.

(32) Teets, T. S.; Labinger, J. A.; Bercaw, J. E. A Thermodynamic Analysis of Rhenium(I)-Formyl C–H Bond Formation via Base-Assisted Heterolytic H_2 Cleavage in the Secondary Coordination Sphere. *Organometallics* **2013**, *32*, 5530–5545.

(33) Jana, R.; Chakraborty, S.; Blacque, O.; Berke, H. Manganese and Rhenium Formyl Complexes of Diphenylphosphine Ligands: Stabilization of the Formyl Unit from Intramolecular B–O Bond Formation. *Eur. J. Inorg. Chem.* **2013**, *2013*, 4574–4584.

(34) Warren, J. J.; Tronic, T. A.; Mayer, J. M. Thermochemistry of Proton-Coupled Electron Transfer Reagents and Its Implications. *Chem. Rev.* **2010**, *110*, 6961–7001.

(35) Morris, R. H. Brønsted–Lowry Acid Strength of Metal Hydride and Dihydrogen Complexes. *Chem. Rev.* **2016**, *116*, 8588–8654.

(36) Karkamkar, A.; Parab, K.; Camaioli, D. M.; Neiner, D.; Cho, H.; Nielsen, T. K.; Autrey, T. A Thermodynamic and Kinetic Study of the Heterolytic Activation of Hydrogen by Frustrated Borane–Amine Lewis Pairs. *Dalton Trans.* **2013**, *42*, 615–619.

(37) Werkmeister, S.; Junge, K.; Beller, M. Catalytic Hydrogenation of Carboxylic Acid Esters, Amides, and Nitriles with Homogeneous Catalysts. *Org. Process Res. Dev.* **2014**, *18*, 289–302.

(38) Dub, P. A.; Ikariya, T. Catalytic Reductive Transformations of Carboxylic and Carbonic Acid Derivatives Using Molecular Hydrogen. *ACS Catal.* **2012**, *2*, 1718–1741.

(39) Kaljurand, I.; Kütt, A.; Soovali, L.; Rodima, T.; Mäemets, V.; Leito, I.; Koppel, I. A. Extension of the Self-Consistent Spectrophotometric Basicity Scale in Acetonitrile to a Full Span of 28 pK_a Units: Unification of Different Basicity Scales. *J. Org. Chem.* **2005**, *70*, 1019–1028.

(40) Bhattacharya, M.; Sebaghi, S.; VanderLinden, R. T.; Saouma, C. T. Toward Combined Carbon Capture and Recycling: Addition of an Amine Alters Product Selectivity from CO to Formic Acid in Manganese Catalyzed Reduction of CO_2 . *J. Am. Chem. Soc.* **2020**, *142*, 17589–17597.

(41) Vollmer, M. V.; Ye, J.; Linehan, J. C.; Graziano, B. J.; Preston, A.; Wiedner, E. S.; Lu, C. C. Cobalt-Group 13 Complexes Catalyze CO_2 Hydrogenation via a $\text{Co}(\text{-I})/\text{Co}(\text{I})$ Redox Cycle. *ACS Catal.* **2020**, *10*, 2459–2470.

(42) Sullivan, B. P.; Meyer, T. J. Kinetics and Mechanism of Carbon Dioxide Insertion Into a Metal–Hydride Bond. A Large Solvent Effect and an Inverse Kinetic Isotope Effect. *Organometallics* **1986**, *5*, 1500–1502.

(43) Kaczmarczyk, E.; Wróbel, R.; Liwo, A.; Chmurzyński, L. Temperature Dependence of the Acid–Base Equilibrium Constants of Substituted Pyridine N-Oxides in Acetonitrile. *J. Mol. Struct.* **1999**, *477*, 113–118.

(44) Gagliardi, L. G.; Castells, C. B.; Rosés, M.; Ràfols, C.; Bosch, E. Acid–Base Dissociation Constants of *o*-Phthalic Acid in Acetonitrile/Water Mixtures over the (15 to 50) °C Temperature Range and Related Thermodynamic Quantities. *J. Chem. Eng. Data* **2010**, *55*, 85–91.

(45) Bratsch, S. G. Standard Electrode Potentials and Temperature Coefficients in Water at 298.15 K. *J. Phys. Chem. Ref. Data* **1989**, *18*, 1–21.

(46) Ellis, W. W.; Ciancanelli, R.; Miller, S. M.; Raebiger, J. W.; DuBois, M. R.; DuBois, D. L. Thermodynamic Hydride Donor Abilities of $[\text{HW}(\text{CO})_4\text{L}]^-$ Complexes ($\text{L} = \text{PPH}_3$, $\text{P}(\text{OMe})_3$, CO) and Their Reactions with $[\text{C}_5\text{Me}_5\text{Re}(\text{PMe}_4)(\text{NO})(\text{CO})]^+$. *J. Am. Chem. Soc.* **2003**, *125*, 12230–12236.

(47) Ilie, S.; Al Herz, A.; Musgrave, C. B.; Glusac, K. D. Thermodynamic and Kinetic Hydricities of Metal-Free Hydrides. *Chem. Soc. Rev.* **2018**, *47*, 2809–2836.

(48) Fukuzumi, S.; Suenobu, T. Hydrogen Storage and Evolution Catalysed by Metal Hydride Complexes. *Dalton Trans.* **2013**, *42*, 18–28.

(49) Kaljurand, I.; Rodima, T.; Pihl, A.; Mäemets, V.; Leito, I.; Koppel, I. A.; Mishima, M. Acid–Base Equilibria in Nonpolar Media. 4. Extension of the Self-Consistent Basicity Scale in THF Medium. Gas-Phase Basicities of Phosphazenes. *J. Org. Chem.* **2003**, *68*, 9988–9993.

(50) Fukuzumi, S.; Ohkubo, K.; Tokuda, Y.; Suenobu, T. Hydride Transfer from 9-Substituted 10-Methyl-9,10-Dihydroacridines to Hydride Acceptors via Charge-Transfer Complexes and Sequential Electron–Proton–Electron Transfer. A Negative Temperature Dependence of the Rates. *J. Am. Chem. Soc.* **2000**, *122*, 4286–4294.

(51) Zhu, X. Q.; Zhang, J. Y.; Cheng, J. P. Negative Kinetic Temperature Effect on the Hydride Transfer from NADH Analogue BNAH to the Radical Cation of N-Benzylphenothiazine in Acetonitrile. *J. Org. Chem.* **2006**, *71*,

7007–7015.

(52) Kaljurand, I.; Koppel, I. A.; Kütt, A.; Rõõm, E. I.; Rodima, T.; Koppel, I.; Mishima, M.; Leito, I. Experimental Gas-Phase Basicity Scale of Superbasic Phosphazenes. *J. Phys. Chem. A* **2007**, *111*, 1245–1250.

(53) Kisanga, P. B.; Verkade, J. G. PK_a Measurements of $P(RNCH_2CH_3)_3N$. *J. Org. Chem.* **2000**, *65*, 5431–5432.

(54) Gennaro, A.; Isse, A. A.; Vianello, E. Solubility and Electrochemical Determination of CO_2 in Some Dipolar Aprotic Solvents. *J. Electroanal. Chem.* **1990**, *289*, 203–215.

(55) Kozuch, S.; Shaik, S. How to Conceptualize Catalytic Cycles? The Energetic Span Model. *Acc. Chem. Res.* **2011**, *44*, 101–110.

(56) Aledo, J. C.; Jiménez-Riveres, S.; Tena, M. The Effect of Temperature on the Enzyme-Catalyzed Reaction: Insights from Thermodynamics. *J. Chem. Educ.* **2010**, *87*, 296–298.

TOC Graphic

